

Submitted to the Astronomical Journal

The Multitude of Molecular Hydrogen Knots in the Helix Nebula ¹

Margaret Meixner and Peter McCullough

Space Telescope Science Institute, 3700 San Martin Drive, Baltimore, MD 21218

meixner@stsci.edu, pmcc@stsci.edu

Joel Hartman

Harvard-Smithsonian Center for Astrophysics, 60 Garden St., Cambridge, MA 02138

jhartman@cfa.harvard.edu

Minho Son

Department of Physics and Astronomy, Johns Hopkins University, Baltimore, MD 21218

mhson@pha.jhu.edu

and

Angela Speck

Dept. of Physics, University of Missouri, Columbia, MO,

speckan@missouri.edu

ABSTRACT

We present HST/NICMOS imaging of the H₂ 2.12 μ m emission in 5 fields in the Helix Nebula ranging in radial distance from 250–450'' from the central star. The images reveal arcuate structures with their apexes pointing towards the central star. These molecular hydrogen knots are most highly structured in the fields closest to the central star and become increasingly less structured with increasing radius. Comparison of these images with comparable resolution ground based images reveals that the molecular gas is more highly clumped than the ionized gas line tracers. From our images, we determine an average number density of knots in the molecular gas ranging from 162 knots/arcmin² in the denser regions to 18 knots/arcmin² in the lower density outer regions. The decreasing number

density of H₂ knots in the outer regions creates a lower filling factor of neutral and molecular gas emission in the radio observations of CO and HI and may explain why these outer regions, where we clearly detect H₂ 2.12 μm, fall below the detection limit of the radio observations. Using this new number density, we estimate that the total number of knots in the Helix to be ~23,000 which is a factor of 6.5 larger than previous estimates. The total neutral gas mass in the Helix is 0.35 M_⊙ assuming a mass of ~ 1.5 × 10⁻⁵ M_⊙ for the individual knots. The H₂ emission structure of the entire Helix nebula supports the recent interpretation of the Helix as a nearly pole-on poly-polar planetary nebula. The H₂ intensity, 5-9 × 10⁻⁵ erg s⁻¹ cm⁻² sr⁻¹, remains relatively constant with projected distance from the central star suggesting a heating mechanism for the molecular gas that is distributed almost uniformly in the knots throughout the nebula. The temperature and H₂ 2.12 μm intensity of the knots can be approximately explained by photodissociation regions (PDRs) in the individual knots; however, theoretical PDR models of PN under-predict the intensities of some knots by a factor of 10. The brightest H₂ emission (~ 3 × 10⁻⁴ erg s⁻¹ cm⁻² sr⁻¹) may be enhanced by a larger than unity area filling factor of H₂ knots or may be an individual H₂ knot exposed to direct starlight causing rapid photoevaporation compared with the more embedded knots of the disk.

Subject headings: planetary nebulae: individual(NGC 7293)

1. INTRODUCTION

Approximately 50 planetary nebulae (PNs) are presently known to have "small scale" heterogeneities located inside or outside the main ionized nebulae (Gonçalves et al. 2001). Cometary knots are a subcategory of small scale structures found commonly in nearby, evolved PNs (O'Dell et al. 2002). Because of its closest proximity (213 parsecs Harris et al. (1997)), the Helix Nebula (NGC 7293) is the best case to study the structure and excitation conditions of cometary knots. The nature of the cometary knots in the Helix was first established by Meaburn et al. (1992). The detailed structure of the cometary knots has been resolved in ionized gas lines in the optical by O'Dell & Handron (1996) with further

¹Based in part on observations with the NASA/ESA Hubble Space Telescope, obtained at the Space Telescope Science Institute, which is operated by the Association of Universities for Research in Astronomy, Inc., under NASA Contract No. NAS 5-26555.

detailed analysis by Burkert & O’Dell (1998), and O’Dell et al. (2000). The emerging optical picture of the cometary knots reveals that they are neutral gas condensations that appear as comet like structures with rims bright in $H\alpha$ and tails that appear as shadows in $[OIII]$ and that point away from the central star. The rim of low-excitation ionize gas has a steep temperature gradient indicating that the knots are photo-evaporating and that ionization fronts are advancing into the knots (O’Dell et al. 2000). A recent anlyasis of knots over the whole Helix nebula by O’Dell et al. (2004) revealed a new 3-D picture for the main ring of the Helix: it is composed of a disk structure and an outer ring tilted almost perpendicularly with respect to the disk. Within each of these components, they observed a similar, progressive evolution in the structure of the knots. The knots closest to the central star and clearly inside of the ionization front were elegantly carved with the brightest rims. The knots furthest from the central star appeared slightly more amorphous in their structure with less well defined rims. The culmination of these optical observations appear to support the theory that these knots were initially formed earlier by instabilities at the ionization front or perhaps by the interaction of the fast stellar wind and then have been sculpted by interaction with the harsh radiation field of the central star (Capriotti 1973).

In contrast to the high angular resolution ($\sim 0.01''$) optical studies of the ionized gas lines in the cometary knots, the molecular gas observations have had lower angular resolution ($4''-41''$) and sensitivity making it difficult to determine the detailed structure and excitation of the main gas component of the cometary knots. These low resolution studies have revealed that the Helix has retained a significant amount of molecular gas (Young et al. 1999; Huggins & Healy 1986; Speck et al. 2002) and that the molecular gas appears to be very clumpy and is probably confined to cometary knot structures (Speck et al. 2002; Huggins et al. 2002). The only detailed study of an isolated cometary knot, which is close to the central star, shows no evidence for large velocities in the molecular gas, ruling out a stellar wind shaping the knot, and reveals a stratified structure for the ionized and molecular gas emissions that is expected in a photodissociation region (PDR) (Huggins et al. 2002). However, since recent optical studies show an evolution of the knot structure with radial distance from the central star (O’Dell et al. 2004), it is not clear that this single knot study is representative of all the knots in the nebula. In order to determine the structure and excitation of the H_2 emission in the cometary knots at comparable resolution to optical images across the Helix, we pursued high angular resolution ($\sim 0.2''$) NICMOS/NIC3 F212N H_2 images at several locations in the nebula, in parallel with the HST/ACS program recently published by O’Dell et al. (2004).

The remainder of this paper is organized as follows. In section 2, we report the observation and data processing procedures. In section 3, we discuss the major observational results and how these relate to the optical ionized gas line emissions imaged by O’Dell et al. (2004). In section 4, we interpret the observations in the context of current understanding

of the Helix’s 3-D structure and discuss the number density, mass, evolution and excitation of the knots as revealed by our H₂ images. We summarize our conclusions in section 5.

2. OBSERVATIONS

The Hubble Helix project (GO program 9700; PI: M. Meixner) imaged the Helix nebula during the 2002 Leonids meteor shower that presented a risk to the HST. The imaging involved a 9 panel mosaic of the Helix using the ACS WFC instrument in the F658N filter (transmitting equally well both the H α 6563 Å and [N II] 6584 Å lines) and the F502N filter (dominated by the [O III] 5007 Å line). In parallel with the ACS imaging, we used NICMOS (Thompson et al. 1998) to image 7 of the possible 9 field positions, 5 of which landed on the nebula (positions 1, 2, 3, 4 and 5) and 2 of which were off the nebula (positions 7 and 9) and used for background measurements for the 5 fields on the nebula. Figure 1 shows the location of these fields on the Helix and the RA and Dec of the field centers for field positions 1, 2, 3, 4, and 5 are listed in Table 1. These parallel NICMOS field positions had insignificant overlap with the the ACS images. Because we wanted maximum field of view and our target was a diffuse nebula, we used the NIC3 camera, 0'2 pixel⁻¹, with the F212N filter to image the H₂ 2.12 μ m line emission in the nebula. For field positions 1 and 2, half the time was spent in the Pa α filter F187N that is sufficiently low signal-to-noise as to be useless and is not discussed further. For each field position, the two dither positions for ACS resulted in two slightly overlapping NICMOS/NIC3 images. The NIC3 MULTIACCUM, FAST readout mode was used. The Hubble Helix project and its results (McCullough & Hubble Helix Team 2002) immediately went into the public domain. The ACS images were analyzed in combination with ground based CTIO images in similar filters and have been published by O’Dell et al. (2004). In this work we analyze and discuss the NICMOS H₂ 2.12 μ m emission and its relation to the ionized gas at high spatial resolution.

The NICMOS/NIC3 images were reduced and calibrated using the standard set of NICMOS calibration programs provided in the latest version (Version 3.1) of IRAF/STSDAS². The CALNICA calibration routines in STSDAS perform zero-read signal correction, bias subtraction, dark subtraction, detector non-linearity correction, flat-field correction, and flux calibration. The pedestal effect was removed by first manually inserting the STSDAS task *biaseq* in the middle of the CALNICA processes (before flat-fielding) and then employing the STADAS task *pedsub* after the CALNICA processes. Cosmic rays were identified and replaced by the median filtered pixel value.

²STSDAS is a product of the Space Telescope Science Institute, which is operated by AURA for NASA

The four dither positions for field positions 7 and 9 were combined to make a “sky” image that is completely attributed to the telescope emission. This “sky” was subtracted from each of the dither frames for field positions 1 – 5 resulting in a H₂ dominated emission frame. The continuum emission from the Helix nebula in the F212N filter is negligible in the sky-subtracted images as demonstrated by Speck et al. (2002). The two dither positions for each field position were combined using drizzle which magnifies the images by a factor of 2. The final drizzled images have a plate scale of 0''.10 pixel⁻¹ and have been rotated so that north is up and east is to the left. Total integration times for the final, drizzled F212N images ranged from 768 seconds for field positions 1 and 2 to 1792 seconds for field position 3. Figures 2, 3, 4, 5 and 6 show the final NICMOS images for field positions 1, 2, 3, 4 and 5, respectively, in comparison with the optical emission line images from O’Dell et al. (2004). These final NICMOS images, in units of count rate per pixel, are available at the MAST web site under the Hubble Helix project.

In order to discern the relative distribution of the H₂ line emission with the ionized gas line tracers, we compare our results with comparable resolution optical images. The overlap between the NICMOS fields and the ACS fields is insignificant. Fortunately, O’Dell et al. (2004) presented ground based CTIO images of H α /[NII], [OIII], H β and [SII] of the entire Helix Nebula at comparable resolution to our NICMOS images. We registered these CTIO images to the WCS of the NICMOS images. The initial comparison, using just the absolute coordinates of the NICMOS and CTIO images, permitted a close enough alignment to identify at least 1 star in common between the NICMOS and CTIO images that was used for translational alignment. The four CTIO images had 6–7 stars in common with each other and our detailed comparison revealed small rotational errors between them up to 0.08° relative angular rotations. Using the star in common with the NICMOS image as the “origin”, we improved the relative rotational alignment of the CTIO images to better than 0.005°. The CTIO images were then translated to the NICMOS WCS position, by aligning the star in common using the task “register” in IRAF. Only the part of the CTIO images that overlap with the NICMOS field positions are shown.

For each field position, we selected a prominent H₂ knot, labeled with a cross in the figures, for surface brightness measurements of the H₂ emission and made a cross-cut along the radial direction from the central star in order to quantify the relation between H₂ emission and distance from the central star. These positions and cross-cuts are labeled on Figs. 2–6 and the locations of the H₂ knotss with respect to the field centers are listed in Table 1. Table 2 lists the surface brightness measurements for H₂ and the optical line tracers at the knot position. The average surface brightness of the H₂ knot emission (DN/pixel) was determined for a circular aperture enclosing the brightest part of the H₂ emission (\sim 3 pixel radius centered on the +). We then converted this average into physical units by

multiplying by $2.44929 \times 10^{-18} \text{ erg s}^{-1} \text{ cm}^{-2} \text{ \AA}^{-1} \text{ DN}^{-1}$ (DN = counts per second), which is the photometry conversion keyword derived for the NICMOS, NIC3 camera, filter F212N for the 77.1 K detector, appropriate for observations taken after January 2002. Finally, to arrive at the units in Table 2, we multiplied by 212.1 \AA which is the filter bandwidth of the F212N filter, and divided by $2.2350443 \times 10^{-13} \text{ sr}$ which is the solid angle of the $0''.10$ pseudo-pixel. For each of the measured H_2 knots in the NICMOS fields, we measured the surface brightness of the ionized gas emission lines, $\text{H}\alpha$ [NII], [OIII], $\text{H}\beta$ and [SII], in the same way and list the results in Table 2. A conversion factor of 1.66×10^{10} was used to convert ADUs/pixel to photons $\text{s}^{-1} \text{ cm}^{-2} \text{ sr}^{-1}$ for all the CTIO images and then each image was multiplied by its photon energy, $\frac{hc}{\lambda}$ to determine the surface brightness in units of $\text{erg s}^{-1} \text{ cm}^{-2} \text{ sr}^{-1}$, the same as the NICMOS H_2 line measurements. For the cross-cuts shown in Figure 7, we applied the same conversion factors.

3. Results

Figures 2, 3, 4, 5 and 6 compare the NICMOS H_2 $2.12\mu\text{m}$ line emission images to the ionized gas tracers of [OIII], $\text{H}\beta$, $\text{H}\alpha$ /[NII] and [SII] from O’Dell et al. (2004) for the respective field positions 1, 2, 3, 4, and 5. Our NIC3 images have better sensitivity and angular resolution than the image in the Speck et al. (2002) and we observe H_2 line emission at much larger distances than seen in their large scale, ground based mosaic. The NICMOS field positions 1 and 2 lie closer to the central star at approximately the same projected distance. The field position 3 follows next in radial distance with positions 5 and 4 overlapping at the farthest radial distances (Fig. 7). In all of the NICMOS field positions the H_2 emission is highly structured revealing arcs and pillars of emission that point towards the central star (Figures 2 – 6). This highly structured appearance contrasts with the more smooth, and less structured appearance of the ionized lines. This difference indicates that the H_2 line emission is confined to the high density neutral gas of the cometary knots (O’Dell & Handron 1996). On the other hand, the ionized gas emission arises from both the more diffuse nebula (50 cm^{-3}) and the cometary knots. Closer inspection of all 5 positions reveals that the $\text{H}\beta$ emission structures correlates very well with the structures observed in H_2 . The [SII] emission appears to correlate with the H_2 emission in positions 1 and 2, but does not show the structure as well as the $\text{H}\beta$. This suggests that the [SII] emission is more extended, diffuse or less defined by the cometary knots. The $\text{H}\alpha$ [NII], which appears like a combination of the $\text{H}\beta$ and [SII] emission, follows the H_2 emission but is much more diffuse in appearance than the H_2 or $\text{H}\beta$.

In positions 1 and 2, the uniformity of the [OIII] emission is punctuated by dark shadows

of cometary knots that appear clearly in H_2 emission. The H_2 knots must lie in front of some highly ionized gas emitting in order to cause the extinction of the [OIII] emission. The fact that most of the H_2 knots do not appear as [OIII] shadows indicates that most of the H_2 knots are confined within the neutral disk and below the highly ionized, diffuse gas apparent in [OIII] emission. The [OIII] emission trails off in intensity in positions 3 and 4 having a diffuse and streaked appearance with no cometary knot emission. The [OIII] emission at these more distant positions probably arises from above the disk. The bright streams of emission in the [OIII] line may be examples of the crepuscular rays found on the large scale [OIII] emission by O’Dell et al. (2004).

The combined cross-cuts (Fig. 7) dramatically show the difference between the H_2 emission and optical line ionized gas tracers. The ionized gas tracers appear to smoothly drop with increasing radius. Differences in the intensity vs. radial distance for these ionized gas tracers are due to the photo-ionization structure of the Helix (O’dell 1998; O’Dell et al. 2004). Of all the ionized gas tracers shown, the $H\beta$ profiles reveal some clumped structure at the 5-10% level on its basically smooth profile. In contrast, the H_2 emission appears to almost randomly fluctuate with radial distance because of the highly clumped, knot structure of the H_2 emission. The H_2 intensity does not appear to decrease significantly with radial distance because the individual knots have a small range of intensities. Positions that overlap in radial distance, 1 & 2 and 4 & 5, are offset in their optical line emissions because they are located at very different azimuthal positions and the nebula has a distinct variation with azimuthal angle. Interestingly, the H_2 emission does not appear to have offsets in emission in the overlap regions further supporting that the H_2 emission appears to have an almost constant level with radial distance.

Detailed comparison of line intensities of the brighter knots in each field position also support this contrast between optical ionize gas emission and H_2 emission. Table 2 lists the brightnesses of a small region in each field position shown as a white cross in the Figures 2 – 6. These regions were selected as bright rims of the H_2 knots and hence measure the brightest H_2 emission in the fields. Our NICMOS images were taken farther out in the Helix nebula into regions that were below the detection limit of Speck et al. (2002), $\sim 10^{-4}$ erg s $^{-1}$ cm $^{-2}$ sr $^{-1}$, and hence complement their picture. The H_2 emission from the bright H_2 clumps decreases by a factor of two between the nearest (pos1) and most distant (pos5) clumps. In comparison, the ionized line emission drops more steeply with the $H\beta$ emission dropping by a factor of 4 and the [OIII] line dropping by a factor of 5.

4. Discussion

4.1. The H₂ nebular structure

Speck et al. (2002) imaged the entire Helix nebula in H₂ showing that it followed the rest of the gas mass tracers and interpreted the H₂ as arising in knots in the main disk of the nebula. However, in their recent analysis of the ACS and CTIO data in combination with velocity data from the literature, O’Dell et al. (2004) revealed an entirely new 3-D structure of the Helix nebula in which the main ring is broken into an inner disk and an outer ring that are almost perpendicular with respect to each other ($\sim 78^\circ$). It is the superposition of these two rings that gives the Helix its helical appearance. Similar multiple axis structures have been observed easily in edge-on poly-polar planetary nebulae such as NGC 2440 (Lopez et al. 1998); however, the almost pole-on view of the Helix has made it more difficult to define its geometry. How does the full-nebula H₂ image of Speck et al. (2002) fit into this new paradigm for the Helix?

Figure 8 shows the inner disk and outer ring structures discussed by O’Dell et al. (2004) superposed on the near-IR H₂ image of Speck et al. (2002). The H₂ near-IR emission of the inner disk is more cleanly separated from the outer ring structure than is found in the optical line tracers and supports the conclusion that the inner disk is a separate structure than the outer ring (O’Dell et al. 2004). This cleaner separation occurs because the H₂ emission arises only from the knots and thus there is better contrast than for the optical line tracers that are diluted by the diffuse emission. The H₂ emission arises at the outer edge of the inner disk that is filled with higher excitation ionized gas, as traced by [OIII], in the center (O’Dell et al. 2004). The H₂ emission arising in the inner disk is also much fainter than the H₂ emission in the outer ring. The opposite is true for the ionized gas tracers: they are much brighter in the inner disk than the outer ring. This reversal suggests that the molecular gas in the inner disk has been largely photo-dissociated in comparison to the outer ring and, hence, the cometary knots are more evolved in the inner disk.

The outer ring does not appear very ring-like in the H₂ emission, but more like a ring with southern and northern arc-extensions at the eastern and western edges that surround the northwest and southeast “plumes” mentioned by O’Dell et al. (2004). In fact, the H₂ emission appears brightest in these plumes. The CO kinematics suggest that these plumes are coherent structures (Young et al. 1999). One possible explanation is that the outer ring defined by O’Dell et al. (2004) is really part of an outer bipolar structure and the southern and northern arcs are the limb-brightened edges of the bicones in the outer structure. Such an interpretation is in line with the Helix nebula being a poly-polar planetary nebula being viewed pole-on. The edge-on poly-polar PN, NGC 2440, has an inner torus of H₂ emission

and an outer bipolar nebula of H₂ emission with axes of symmetry that are tilted with respect to one another (Latter et al. 1995).

Our NICMOS field positions appear to lie in some of the fainter or non-existent regions of H₂ emission as observed by Speck et al. (2002) which had less sensitivity than our study. Positions 1 and 2 are located outside the southern edge of the inner disk in what appears to be a gap between the inner disk and outer structures. Position 3 lies to the southwest of the outer structure where no apparent H₂ emission appears in the H₂ image by Speck et al. (2002). Positions 4 and 5 are located even further away from previously detectable H₂ emission south of the nebula. Positions 3, 4 and 5 also lie in regions where no HI 21 cm line emission was detected by Rodríguez et al. (2002) nor CO emission detected by Young et al. (1999). The number density of H₂ knots and area filling factor of H₂ emission decreases with increasing radius and is the lowest in positions 3, 4 and 5 (Figs. 4 – 6). In the large beams of these radio line observations ($\sim 31''$ FWHM for CO and $\sim 42''$ FWHM for HI 21 cm), the intensity of the neutral gas emission from these knots is beam diluted and falls below the detection limit of the radio observations.

4.2. The multitude of molecular knots in the Helix

Our observations clearly show that the morphology of the molecular hydrogen emission is highly clumped in comparison to the ionized gas tracers. Figure 9 shows a multi-color image comparing the [OIII], the H α /[NII] and the H₂ emission for position 1. The structure observed in this image is primarily due to the H₂ emission clumps. In fact, the H₂ emission images are striking by their lack of diffuse H₂ emission. Close inspection of the more intense regions shows they are composed of overlapping knots of H₂ emission. Hence, we confirm the conclusion of Speck et al. (2002) that the molecular hydrogen is confined to the high density knots such as seen in the optical by O’Dell & Handron (1996). A similar conclusion was reached by Speck et al. (2003) for the Ring Nebula based on comparison of high resolution ground-based H₂ emission images to the optical HST images. Thus in two evolved planetary nebulae, the Helix and the Ring Nebulae, the H₂ line emission is highly structured and confined to knots.

The near-IR H₂ emission provides us with the highest angular resolution map of the neutral gas knots in the Helix nebula. Previous work has suggested that the knots contain all the neutral gas detected at substantially lower angular resolution in the CO emission ($\sim 31''$ FWHM) by Young et al. (1999), in the CI emission ($\sim 15''$ FWHM) by Young et al. (1997), the HI emission ($\sim 42''$ FWHM) by Rodríguez et al. (2002) and the H₂ line emission ($\sim 4''$ FWHM) by Speck et al. (2002). However, all previous neutral gas studies have had

insufficient resolution and sensitivity to separate and determine the structure and number density of these neutral gas knots. The optical study of the knots by O’Dell & Handron (1996) provided an initial, lower limit for the total number of cometary knots to be 3500 in the entire nebula. They base this estimate by extrapolating the number density of knots they can identify in their WFPC2 optical images vs. radius to the entire nebula. Our H₂ images reveal that many more molecular knots exist as defined by the H₂ emission arcs than can be identified in the optical images (Figures 2 – 6). For example, in the NICMOS field position 1 the number of knots that appear as [OIII] shadows are less than 10; however, the number of arc-shaped H₂ emission structures is ~ 150 . In Table 3, we list the number of knots, which we identify by arcs of H₂ emission, and the FOV of the image. The number density of knots is simply the total divided by the FOV. The area filling factor of H₂ emission is the percentage of the FOV that contains H₂ emission structures above a 1σ threshold intensity ($\sim 1 - 2 \times 10^{-5}$ erg s⁻¹ cm⁻² sr⁻¹). The total number of knots, the number density of knots and the area filling factors are the highest for positions 1 and 2, and decrease with larger radial distance from the star as seen in positions 4 and 5. Interestingly, the peak surface brightness of the knots does not decrease significantly with radial distance as we see in Figure 7 and Table 2.

We estimate the total number of molecular knots in the Helix by scaling the number of knots we observe in our NICMOS images to the total angular size of the Helix. If we look at the H₂ image of Speck et al. (2002) we find that our NICMOS field positions 1 and 2 land in a region of average or slightly below average H₂ intensity. So, we base a conservative estimate of the total number of knots by using the average knot number density of positions 1 and 2, 0.041 knots/arcsec². The H₂ emission region is an annulus with an inner radius of $\sim 170''$ and an outer radius of $450''$ covering a total angular area of 5.5×10^5 arcsec². Multiplying the average knot number density by the total angular area equals $\sim 23,000$ molecular hydrogen knots in the Helix nebula or a factor of 6.5 larger than previous estimates based on optical images (O’Dell & Handron 1996). The estimated mass of a single Helix knot is $\sim 1.5 \times 10^{-5}$ M_⊙ (O’Dell & Handron 1996) or 10^{-4} M_⊙ (Young et al. 1997). However, the Young et al. (1997) CI study defined a “knot” to be the size of $30'' \times 10''$ in size, which would include ~ 10 H₂ knots if we assume the knot densities of position 1. Because our H₂ knots appear similar in shape and size to the optical knots observed by O’Dell & Handron (1996), we adopt their mass estimate for individual knots. If, for simplicity, we assume that all H₂ knots have similar properties with an average mass of $\sim 1.5 \times 10^{-5}$ M_⊙ (O’Dell & Handron 1996), then the total neutral gas mass of the Helix nebula is ~ 0.35 M_⊙. Our neutral gas mass estimate is substantially larger than the 0.01 M_⊙ estimated by O’Dell & Handron (1996) who underestimated the total number of knots. It is also higher than the 0.18 M_⊙ estimated from the CO observations that were corrected for the atomic CI emitting gas by Young et

al. (1999) who have underestimated the mass because the CO observations do not detect all of the molecular gas. Our estimate of the neutral gas mass is comparable to the ionized gas mass of $0.3 M_{\odot}$ (Henry et al. 1999), and the total gas mass in the nebula is $>0.65 M_{\odot}$ in the main part of the disk. The mass loss rate, that created the main disk over $\sim 28,000$ years is $\dot{M} > 2.3 \times 10^{-5} M_{\odot} \text{ y}^{-1}$. Such a large mass loss rate supports the independent conclusion that the Helix’s progenitor star was massive, $6.5 M_{\odot}$, resulting in a present day core mass of $0.93 M_{\odot}$ (Gorny et al. 1997).

4.3. The evolution of H₂ knots

Figure 10 shows a close up of the bright knot in NICMOS field position 1 in three tracers, [OIII], H₂ and H β . The knot extinguishes the [OIII] emission and its long shadow runs off to the bottom left corner. The arc-shaped head of the knot is clearly observed in the H₂ emission and is apparent, at lower contrast, in the H β emission. Close comparison of the molecular hydrogen emission shows that it almost coincides with the H β and is displaced towards the star from the shadowed regions of the the [OIII] absorption of the knot (Fig. 10). This structure suggests that the H₂ emission arises in mini-PDRs on the clump surfaces that point toward the central star. The intensities measured for the H₂ emission are consistent with the PN-PDR models of Natta & Hollenbach (1998). Comparison of this knot structure (Fig. 10) with the detailed study of an optically bright knot in the inner most regions of the Helix (Huggins et al. 2002) reveals a change in the knot’s structure. The most inward knot studied in H₂ by Huggins et al. (2002) is pillar-like with a well developed crown structure. The H α emission in this knot lies closer to the central star compared to the H₂ emission and the H₂ emission lies closer to the central star than the CO emission of the knot. This stratified structure is what we expect for a PDR. However, we do not see a separated stratification of the H₂ and H β emission from our example knot from Position 1. This difference in layered vs. not layered structure of the knots’ PDRs suggest that the inner most knot has a more evolved PDR front than the Position 1 knot.

A comparison of the different field positions shows a progression in the morphology of the H₂ knots with radial distance from the central star. The positions closest to the central star (positions 1 and 2) have numerous knots, with cometary structures, i.e. arcs at the top spires. The farthest positions (4 and 5) have substantially less knots and less structure to the knots. Position 3, which lies in between the two extremes, has a middle density of knots that are lined in continuous rows with fewer spire structures. A similar trend from highly structured to almost amorphous was observed in the H α structure of the knots by O’Dell et al. (2004). The H₂ emission traces this morphological change even further out into the

nebula showing that the neutral gas clumps have even less structure PNs at the outer edge of the nebula. This progression supports the idea that the initial stages of the structure formation is caused by instabilities in the interacting winds front or by the ionization front that are later refined by the photo-excitation.

4.4. The H₂ knots as mini-PDRs

When molecular hydrogen was first imaged in PNs it was found that their brightnesses were too high for the molecular emission to have originated in photo-dissociation regions (PDRs) and thus attributed to shock excitation (Beckwith et al. 1978; Zuckerman & Gatley 1988). However, the PDR models used for these comparisons were designed for interstellar molecular clouds, rather than circumstellar nebulae around rapidly evolving stars. As such these models only included Far-UV photons and failed to include the soft X-ray emission inherent from very hot (>100,000 K) white dwarfs. The temperature of the white dwarf also changes as the star evolves during the lifetime of the PN. Furthermore, the original models assumed that the cloud was homogeneous, while the gas around PNs is clearly very clumpy in structure. In addition, the interstellar clouds are not expanding, whereas this is the case for the gas around PNs, causing a change in the optical depth of the gas and therefore allowing the photons to penetrate the gas more easily. The models of Natta & Hollenbach (1998) included three of these factors (evolving central star, expanding gas, x-ray photons) into their PDR model for PNs, and showed that the molecular hydrogen emission was approximately consistent with excitation of H₂ in PDRs in these environments. The Natta & Hollenbach (1998) model has been applied to three PNs, NGC2346 (Vicini et al 1999), the Helix nebula (Speck et al. 2002), and the Ring Nebula (Speck et al. 2003).

Our new observations of the Helix molecular knots confirms that the PDR gas in the Helix resides in a multitude of mini-PDRs, not in a diffuse molecular component (Speck et al. 2002; Huggins et al. 2002). The other, perhaps more suprising fact is that the intensity of individual knots remains fairly constant with distance from the central star in the range $5-9 \times 10^{-5}$ erg s⁻¹ cm⁻² sr⁻¹ (Table 2; Fig. 7). The apparent, almost random variation in the H₂ line intensity with respect to radius (Fig. 7) occurs because the number density of knots varies along the cross cut not the intensity of the knots themselves. The relative consistency of the H₂ line intensity of the individual knots with respect to distance from the central star further supports that the PDRs are distributed as mini-PDRs and there is not one PDR front for the Helix but a multitude of them. The higher rotational lines of H₂, that were observed with ISOCam by Cox et al. (1998), indicate a thermalized temperature of the gas to be ~900 K that appears to be independent of distance from the central star. The gas

density within the knots, $\sim 10^4 - 10^5 \text{ cm}^{-3}$ is high enough to thermalize the fluorescently excited H_2 gas. The observed H_2 line intensities of the Helix and the derived molecular gas temperature are approximately consistent with the PN/PDR theory of Natta & Hollenbach (1998). For evolution of the most massive stars, e.g. core mass $0.836 M_\odot$, at the age of the Helix, $\sim 16,000$ years, Natta & Hollenbach (1998) predict H_2 gas temperatures of ~ 1000 K and H_2 $2.12 \mu\text{m}$ line intensities of $\sim 5 \times 10^{-5} \text{ erg s}^{-1} \text{ cm}^{-2} \text{ sr}^{-1}$ in good agreement with the observed temperature and the individual H_2 line intensities of the majority of knots. At this stage of the PN PDR evolution, the H_2 line intensity decreases only gradually with time and the heating of the molecular gas is dominated by the soft- X-ray emission of its $123,000$ K central star (Bohlin et al. 1982).

Despite this approximate success of the PN/PDR models of Natta & Hollenbach (1998), these models fall short of complete success. The brightest H_2 intensity is almost a factor of 10 larger than the Natta & Hollenbach (1998) prediction. Recent model calculations of the H_2 intensity of knots in radiative equilibrium with the stellar radiation field by O’Dell et al. (2005) also under-predict the H_2 line intensities. The solution to this underprediction of both models, may be to combine the time evolution aspects of the Natta & Hollenbach (1998) models with the inclusion of knots, as modelled by O’Dell et al. (2005). For example, the time-dependent process of photo-evaporation causes an advection of the H_2 from the surface of the knot and a propagation of the PDR front into the knot which may boost the H_2 emission because of the constant photodissociation of fresh molecular gas (Natta & Hollenbach 1998). Evidence for photoevaporation has been found in the ionized gas studies of the inner most knots (O’Dell et al. 2000), which are knots that are directly exposed to the central star light. Thus, the higher H_2 knots could be those that are directly exposed to the central starlight and experiencing photoevaporation. However, most knots experience a softer starlight that has been attenuated by intervening knots of molecular gas and dust. Secondly, the brightest H_2 intensity detected by Speck et al. (2002), $\sim 3 \times 10^{-4} \text{ erg s}^{-1} \text{ cm}^{-2} \text{ sr}^{-1}$, may be the result of multiple knots along the line of sight, i.e. filling factors greater than 1 that have a multiplying effect on the intensity. This raises an interesting point that the spatial distribution of H_2 over the entire nebula varies not because of substantial H_2 intensity variation, as one might expect in a PDR front. Rather, the apparent H_2 surface brightness is proportional to the number density of H_2 knots.

5. Conclusions

New observations of H_2 $2.12 \mu\text{m}$ line reveal several new aspects to the molecular knots of the Helix nebula. The H_2 images reveal that the knots have arcuate structures with the apex

pointing towards the central star. These molecular hydrogen knots are most highly structured in the field positions closest to the central star and become increasingly less structured with increasing radius. All of the H_2 emission is confined to knots. In contrast the ionized gas tracers have a significant component of diffuse ionized gas emission. Using the number density of molecular hydrogen knots in the 5 NICMOS field positions, we estimate the total number of knots to be $\sim 23,000$, a factor of 6.5 more than previous estimates based on optical images. The total neutral gas mass in the Helix based on these new knots estimates is $0.35 M_\odot$ assuming an average mass of $\sim 1.5 \times 10^{-5} M_\odot$ for the individual knots based on previous work by O’Dell & Handron (1996). The H_2 emission structure of the entire Helix nebula supports the recent interpretation of the Helix as a nearly pole-on poly-polar planetary nebula. The average intensity is $5\text{-}9 \times 10^{-5} \text{ erg s}^{-1} \text{ cm}^{-2} \text{ sr}^{-1}$ remains relatively constant with projected distance from the central star. The temperature and H_2 $2.12 \mu\text{m}$ intensity of the knots suggest an origin in the photodissociation regions (PDRs) of the individual knots; however, theoretical models for the PDRs in planetary nebulae do not adequately reproduce the H_2 intensity. The brightest knots appear in regions of more numerous knots and may be exposed to direct starlight that may cause rapid photoevaporation in comparison to the more embedded knots of the disk.

We gratefully acknowledge the work of many STScI colleagues who contributed to this observational setup of this project. Zoltan Levay who superposed the NICMOS fields on the combined CTIO and ACS image. This work was supported in part by an STScI grant GO 01041 and by the internal STScI funds, DDRF D0001.82319.

REFERENCES

- Beckwith, S., Gatley, I., & Persson, S. E. 1978, *ApJ*, 219, L33
- Bohlin, R. C., Harrington, J. P., & Stecher, T. P. 1982, *ApJ*, 252, 635
- Burkert, A., & O’dell, C. R. 1998, *ApJ*, 503, 792
- Capriotti, E. R. 1973, *ApJ*, 179, 495
- Cox, P., et al. 1998, *ApJ*, 495, L23
- Gonçalves, D. R., Corradi, R. L. M., & Mampaso, A. 2001, *ApJ*, 547, 302
- Gorny, S. K., Stasinska, G., & Tylanda, R. 1997, *A&A*, 318, 256

- Harris, H. C., Dahn, C. C., Monet, D. G., & Pier, J. R. 1997, IAU Symp. 180: Planetary Nebulae, 180, 40
- Henry, R. B. C., Kwitter, K. B., & Dufour, R. J. 1999, ApJ, 517, 782
- Huggins, P. J., Forveille, T., Bachiller, R., Cox, P., Ageorges, N., & Walsh, J. R. 2002, ApJ, 573, L55
- Huggins, P. J., & Healy, A. P. 1986, ApJ, 305, L29
- Kastner, J. H., Gatley, I., Merrill, K. M., Probst, R., & Weintraub, D. 1994, ApJ, 421, 600
- Latter, W. B., Kelly, D. M., Hora, J. L., & Deutsch, L. K. 1995, ApJS, 100, 159
- Lopez, J. A., Meaburn, J., Bryce, M., & Holloway, A. J. 1998, ApJ, 493, 803
- McCullough, P. R., & Hubble Helix Team 2002, American Astronomical Society Meeting Abstracts, 201
- Meaburn, J., Walsh, J. R., Clegg, R. E. S., Walton, N. A., Taylor, D., & Berry, D. S. 1992, MNRAS, 255, 177
- Meixner, M., McCullough, P., Hartman, J., O'dell, R., & Speck, A. K. 2004, Astronomical Society of the Pacific Conference Series, 313, 234
- Natta, A., & Hollenbach, D. 1998, A&A, 337, 517
- O'dell, C. R., & Handron, K. D. 1996, AJ, 111, 1630
- O'dell, C. R. 1998, AJ, 116, 1346
- O'Dell, C. R., Henney, W. J., & Burkert, A. 2000, AJ, 119, 2910
- O'Dell, C. R., Balick, B., Hajian, A. R., Henney, W. J., & Burkert, A. 2002, AJ, 123, 3329
- O'Dell, C. R., McCullough, P. R., & Meixner, M. 2004, AJ, 128, 2339
- O'Dell, C. R., Henney, W. J., & Ferland, G. J 2005, AJ, in press.
- Rodríguez, L. F., Goss, W. M., & Williams, R. 2002, ApJ, 574, 179
- Speck, A. K., Meixner, M., Fong, D., McCullough, P. R., Moser, D. E., & Ueta, T. 2002, AJ, 123, 346
- Speck, A. K., Meixner, M., Jacoby, G. H., & Knezek, P. M. 2003, PASP, 115, 170

Thompson, R. I., Rieke, M., Schneider, G., Hines, D. C., & Corbin, M. R. 1998, *ApJ*, 492, L95

Vicini, B., Natta, A., Marconi, A., Testi, L., Hollenbach, D., & Draine, B. T. 1999, *A&A*, 342, 823

Young, K., Cox, P., Huggins, P. J., Forveille, T., & Bachiller, R. 1999, *ApJ*, 522, 387

Young, K., Cox, P., Huggins, P. J., Forveille, T., & Bachiller, R. 1997, *ApJ*, 482, L101

Zanstra, H. 1955, *Vistas in Astronomy*, 1, 256

Zuckerman, B., & Gatley, I. 1988, *ApJ*, 324, 501

Table 1: NICMOS field position centers and the H₂ knot positions with respect to these centers

Positions	RA(2000) of (0,0) (h m s)	Dec(2000) of (0,0) (° ' ")	ΔRA to H ₂ knot (")	ΔDec to H ₂ knot (")
central star	22 29 38.5	-20 50 13.5		
pos1	22 29 53.03	-20 53 27.87	-28.32	31.57
pos2	22 29 40.23	-20 54 44.07	-34.51	18.68
pos3	22 29 27.44	-20 56 0.26	-4.97	22.53
pos4	22 29 59.67	-20 56 21.79	7.11	41.01
pos5	22 29 44.98	-20 58 10.38	-7.01	35.72

Table 2: Surface Brightnesses of Field Positions

Positions of H ₂ knot	Radius (")	H ₂	Hα/[NII]	Hβ (erg s ⁻¹ cm ⁻² sr ⁻¹)	[OIII] (5007 Å)	[SII] (6725 Å)
pos1	253	1.27365E-04	7.95596E-02	9.33381E-03	4.31994E-02	1.42868E-03
pos2	257	9.38642E-05	8.19865E-02	1.05037E-02	6.45470E-02	1.51075E-03
pos3	360	8.55222E-05	4.51389E-02	9.29548E-03	9.49064E-03	1.09471E-03
pos4	448	8.61214E-05	2.47975E-02	2.90198E-03	6.68796E-03	6.28393E-04
pos5	436	5.99320E-05	2.42383E-02	2.36069E-03	3.43582E-03	6.77509E-04

Table 3: Number of H₂ Knots

Positions	Total	FOV area	number density	area filling factor of H ₂ emission
pos1	150	50"×80"	135 knots/arcmin ²	80%
pos2	180	50"×80"	162 knots/arcmin ²	70%
pos3	90	50"×80"	81 knots/arcmin ²	60%
pos4	90	50"×100"	65 knots/arcmin ²	50%
pos5	20	50"×80"	18 knots/arcmin ²	25%

FIGURE CAPTIONS:

Figure 1: This negative picture of the Helix from O’Dell et al. (2004) shows the optical structure on a large scale. The NICMOS field positions are overlaid as black rectangles.

Figure 2: NICMOS position 1. The observed H_2 $2.12\mu\text{m}$ emission is at the upper right column box, with the [OIII] (top-left), $H\beta$ (right-center), $H\alpha$ /[NII] (right bottom), and [SII] (left bottom) emission from the same region extracted from the CTIO ground based images O’Dell et al. (2004). The white cross (+) marks the location where the flux measurements of Table 2 were taken. The white line shows the location of the crosscut shown in Fig. 7. The approximate direction of the central star is shown with the label.

Figure 3: NICMOS position 2, same as figure 1.

Figure 4: NICMOS position 3, same as figure 1.

Figure 5: NICMOS position 4, same as figure 1.

Figure 6: NICMOS position 5, same as figure 1.

Figure 7: The combined intensity radial profiles of NICMOS positions 1-5 shown as a function of distance from the central star for the different emission line tracers as labeled in the boxes. The top left box shows the horizontal location of the position slices in relative radial distances from the central star. Variations in intensity at the same radial distance but different positions is caused by the azimuthal variation of the nebular intensity emission.

Figure 8: H_2 line emission image from Speck et al. (2002) with the inner disk and outer ring structures labelled as identified by O’Dell et al. (2004).

Figure 9: NICMOS position 1 in three colors representing the H_2 , the $H\alpha$ + [NII] and the [OIII] as shown in the legend. This color comparison re-emphasizes the clumpy nature of H_2 line emission in comparison to the more diffuse ionized gas line emission.

Figure 10: The selected H_2 knot from NICMOS position 1 shown in [OIII] (shadow), H_2 and $H\beta$ line emission. The white cross, which marks the location of the line emission measurement, is a guide for the relative position of these emissions. The H_2 and $H\beta$ line emissions appear spatially coincident while the [OIII] shadow column ends at the cross and the H_2 arc emission structure.

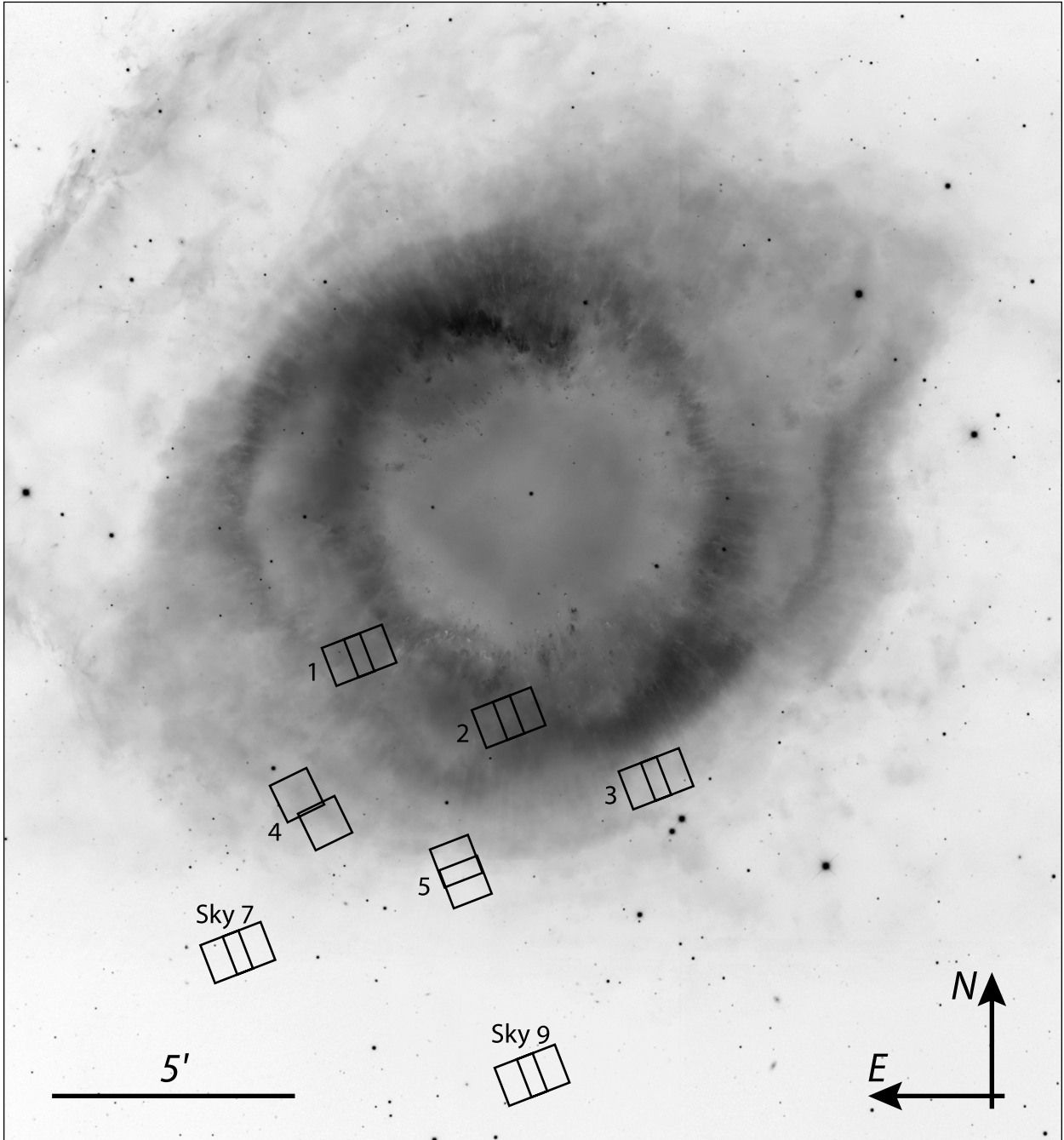


Fig. 1.— This negative picture of the Helix from O’Dell et al. (2004) shows the optical structure on a large scale. The NICMOS field positions are overlaid as black rectangles.

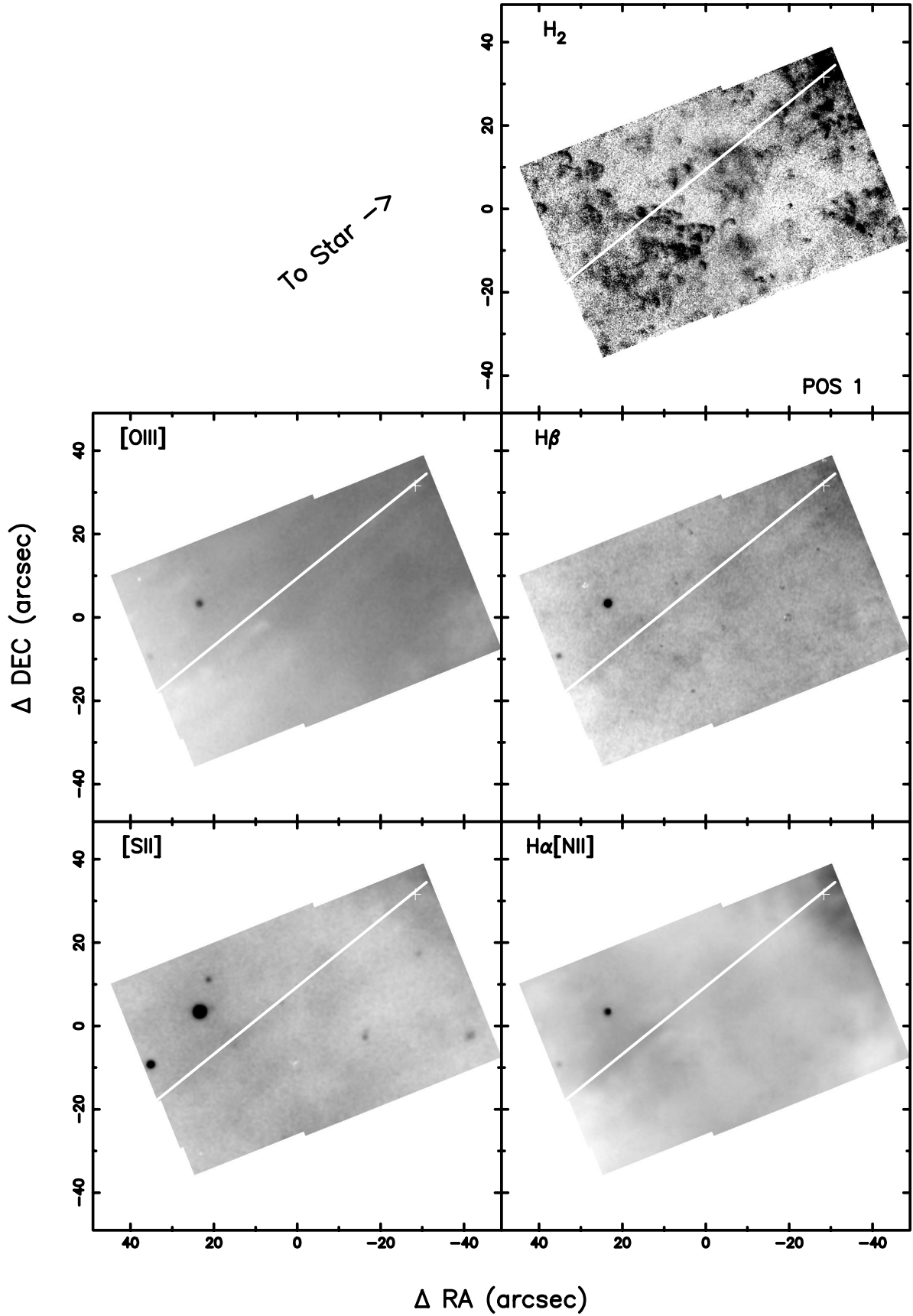


Fig. 2.— NICMOS position 1. The observed H_2 $2.12\mu m$ emission is at the upper right column box, with the $[OIII]$ (top left), $H\beta$ (right center), $H\alpha/[NII]$ (right bottom), and $[SII]$

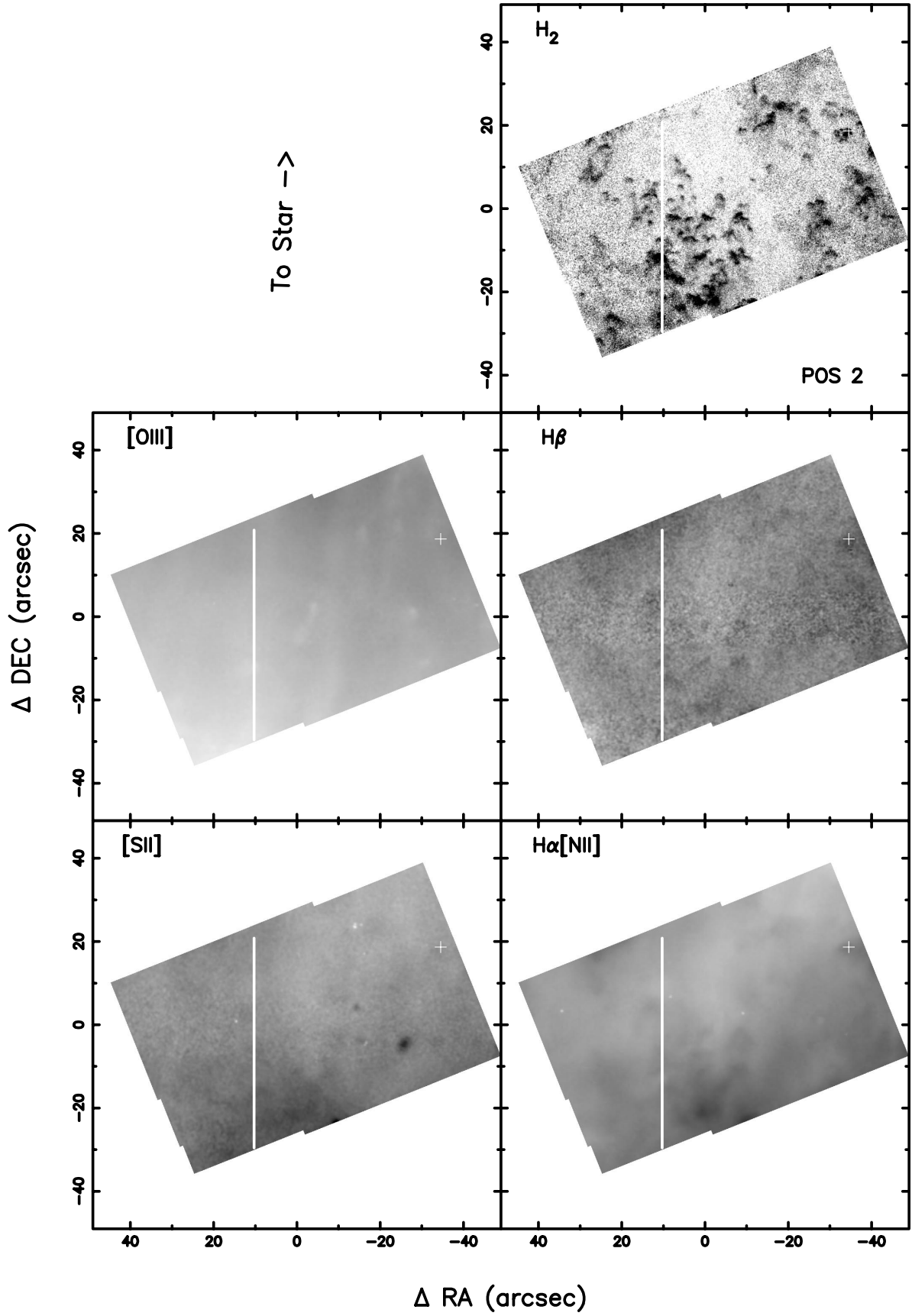


Fig. 3.— NICMOS position 2, same as figure 1.

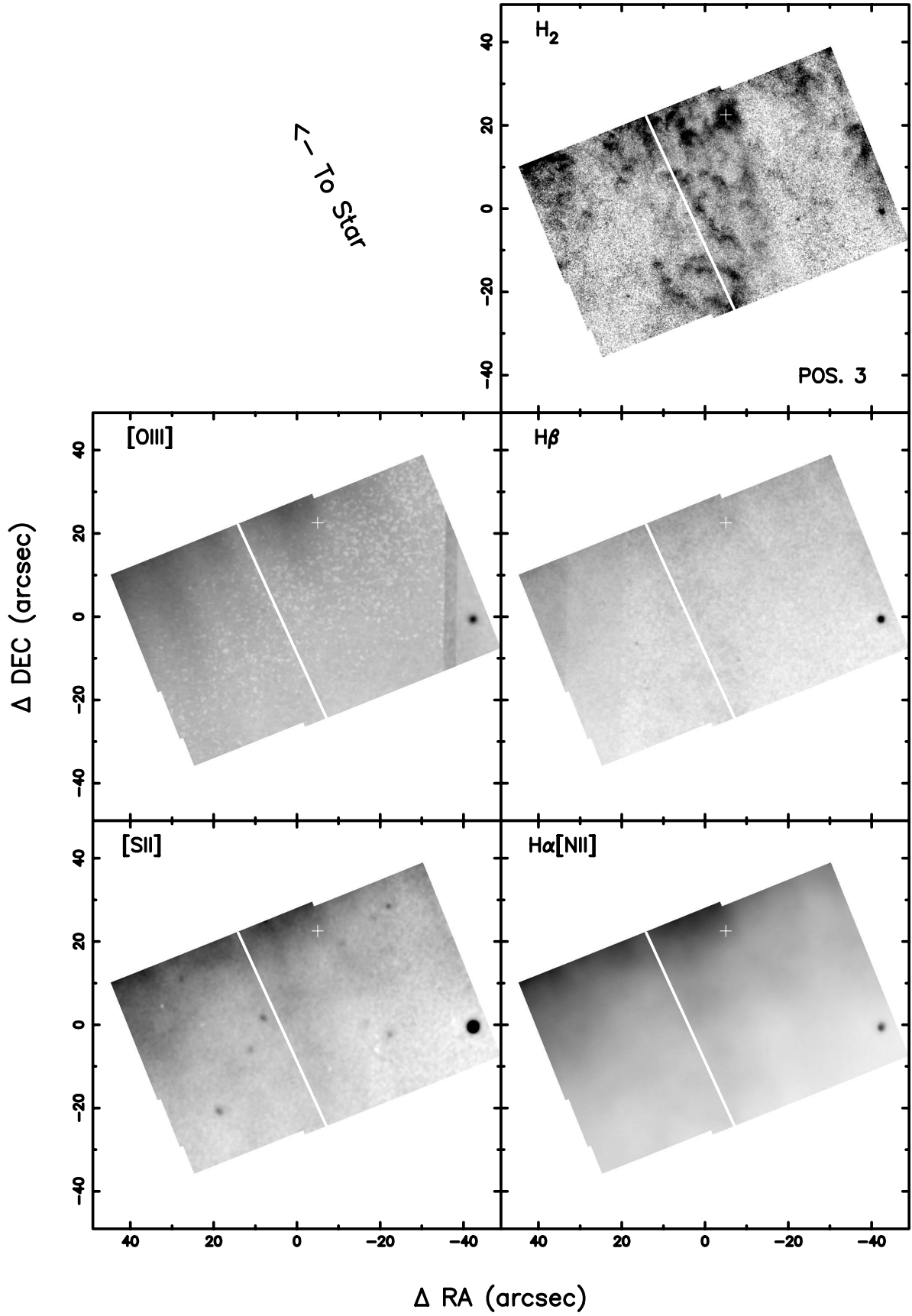


Fig. 4.— NICMOS position 3, same as figure 1.

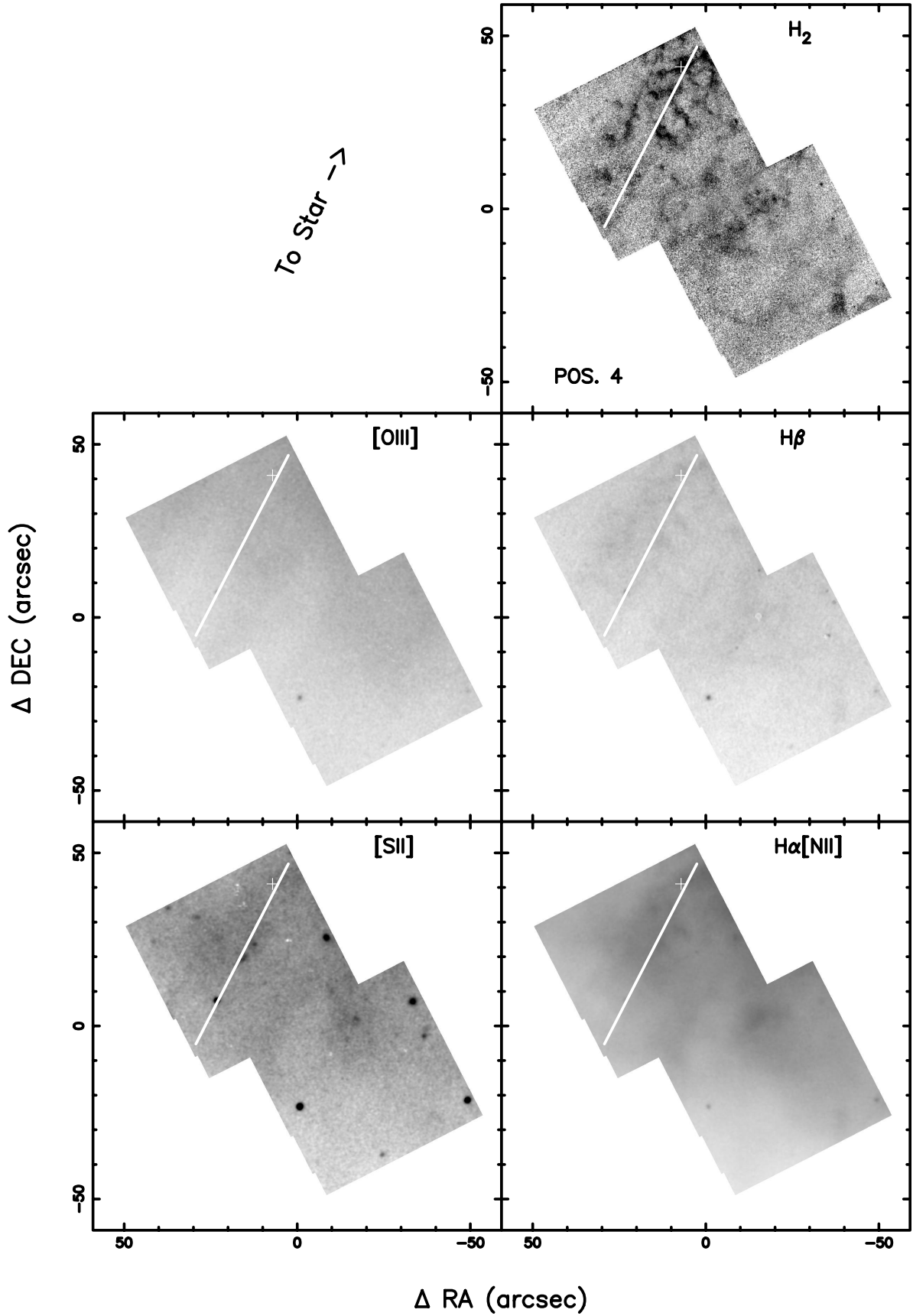


Fig. 5.— NICMOS position 4, same as figure 1.

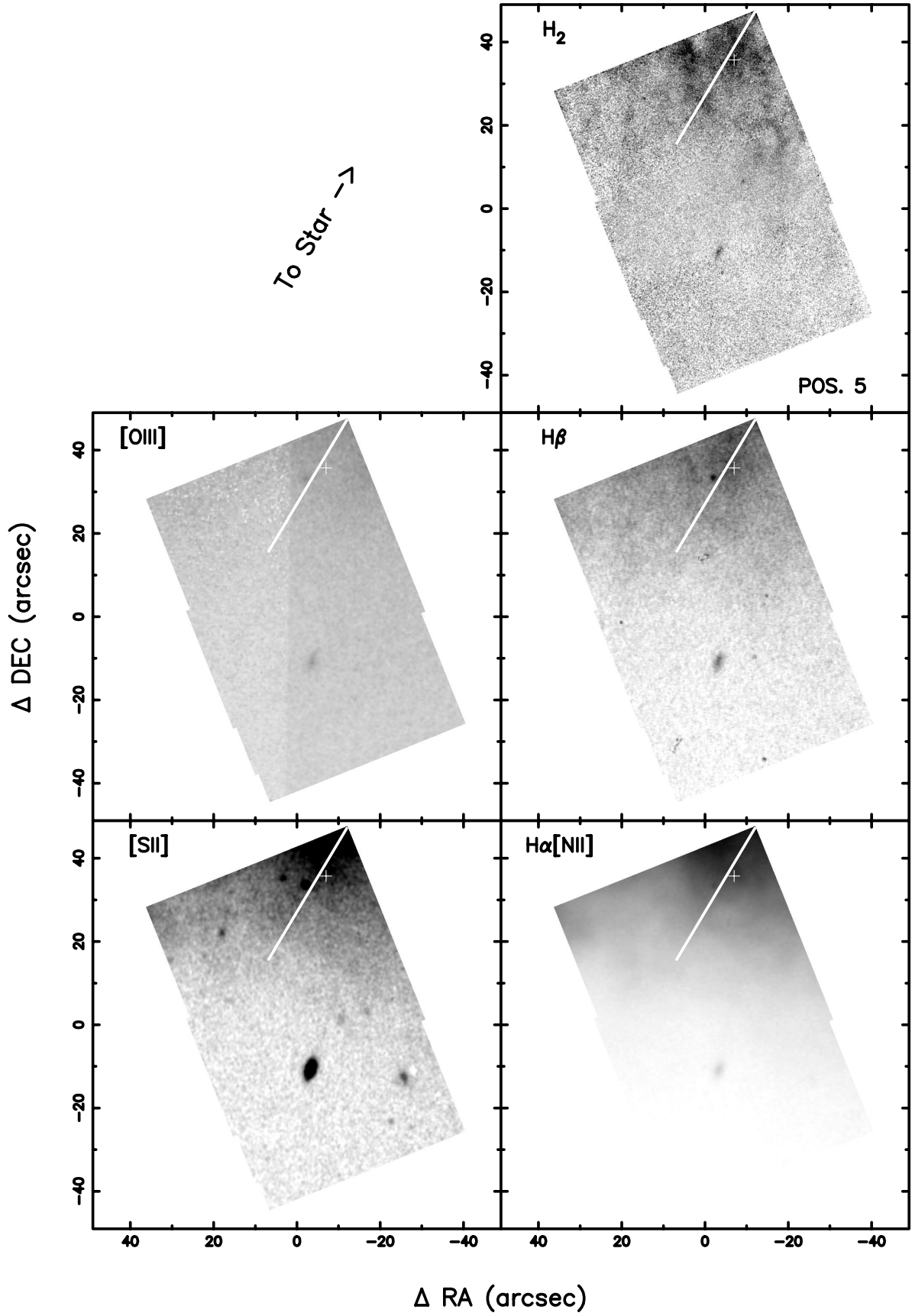


Fig. 6.— NICMOS position 5, same as figure 1.

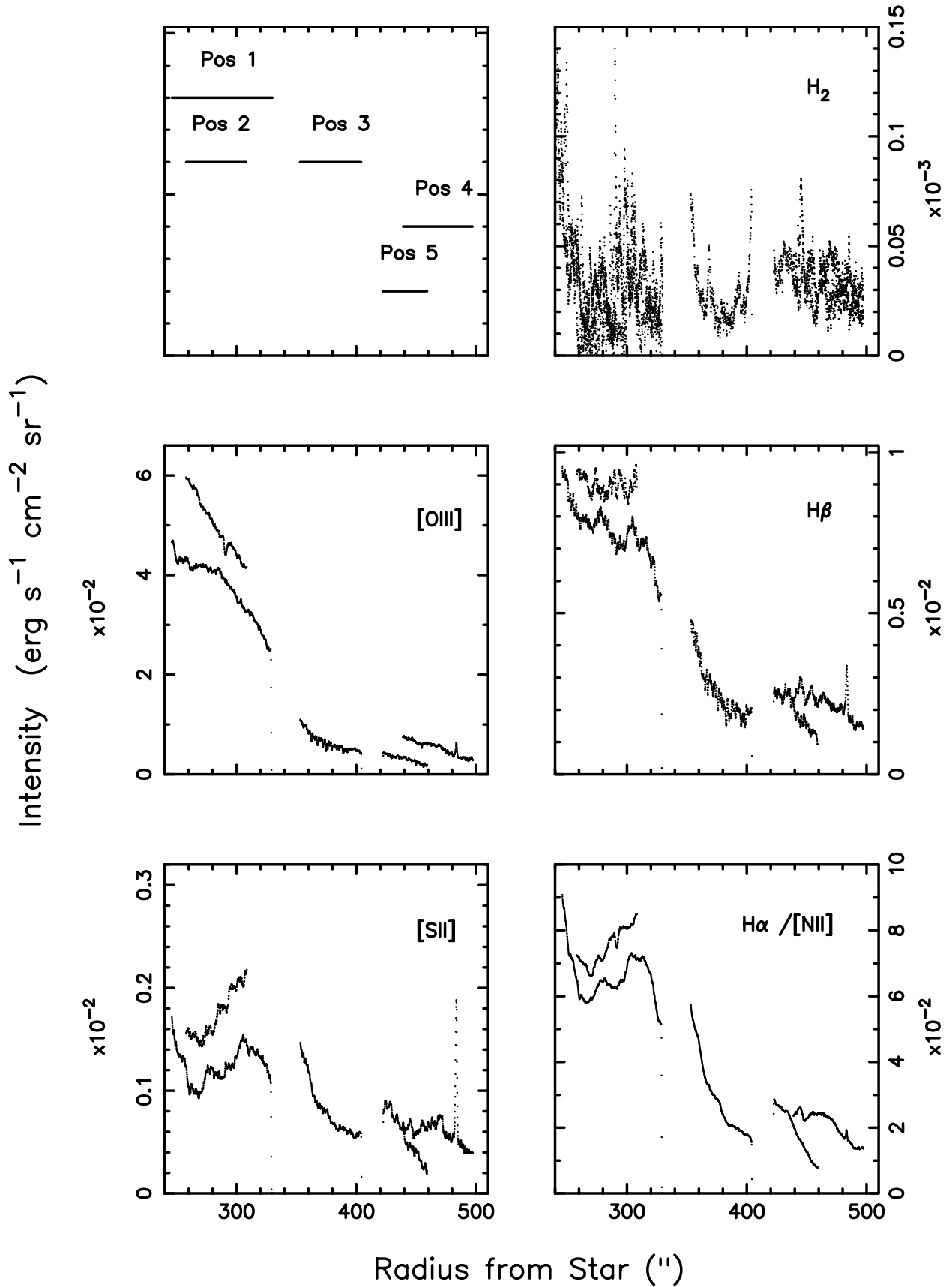


Fig. 7.— The combined intensity radial profiles of NICMOS positions 1-5 shown as a function of distance from the central star for the different emission line tracers as labeled in the

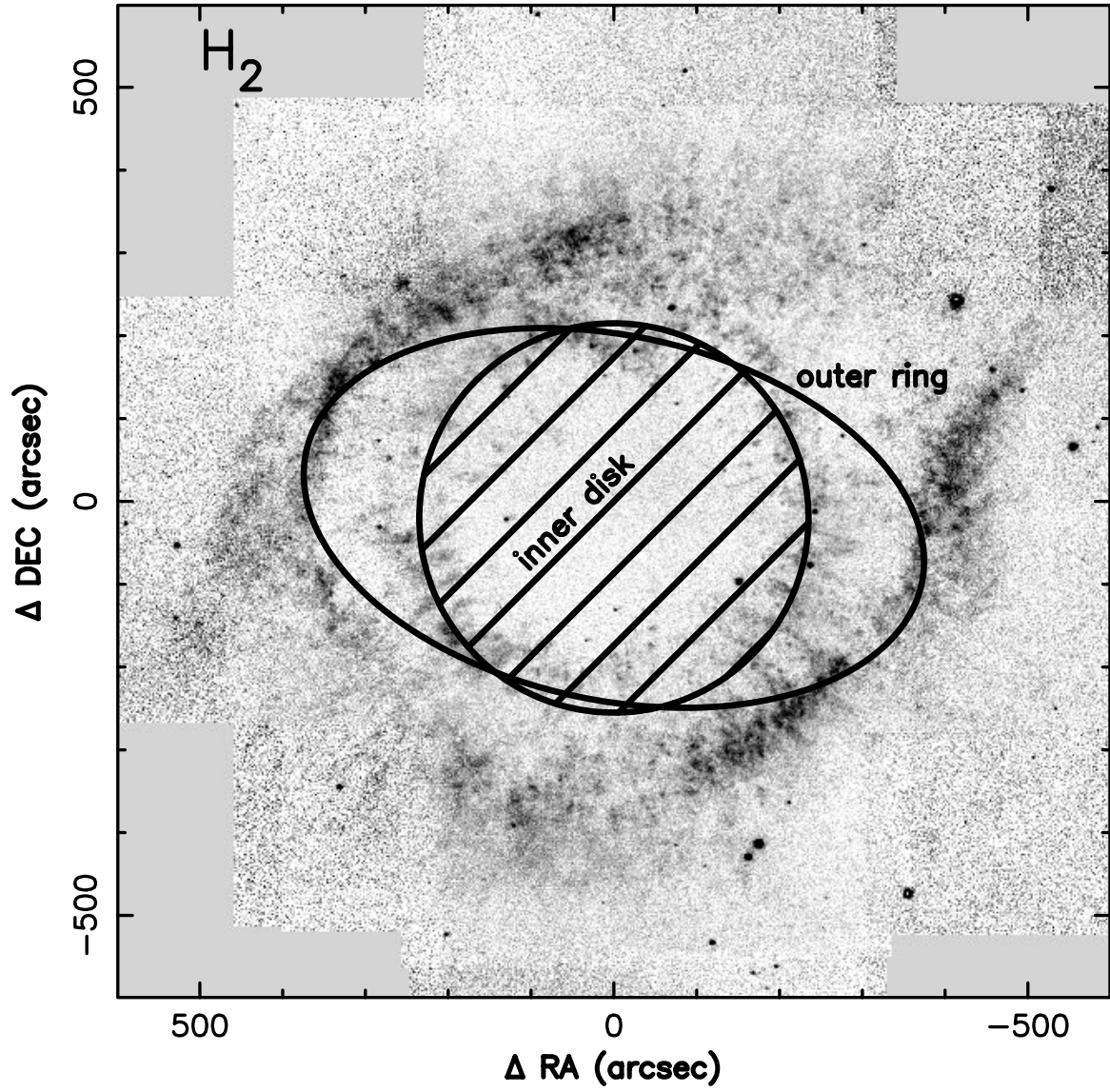


Fig. 8.— H₂ line emission image from Speck et al. (2002) with the inner disk and outer ring structures labelled as identified by O’Dell et al. (2004).

Helix Nebula
NGC 7293

HST NICMOS F212N H₂
CTIO H α + [N II]
CTIO [O III]

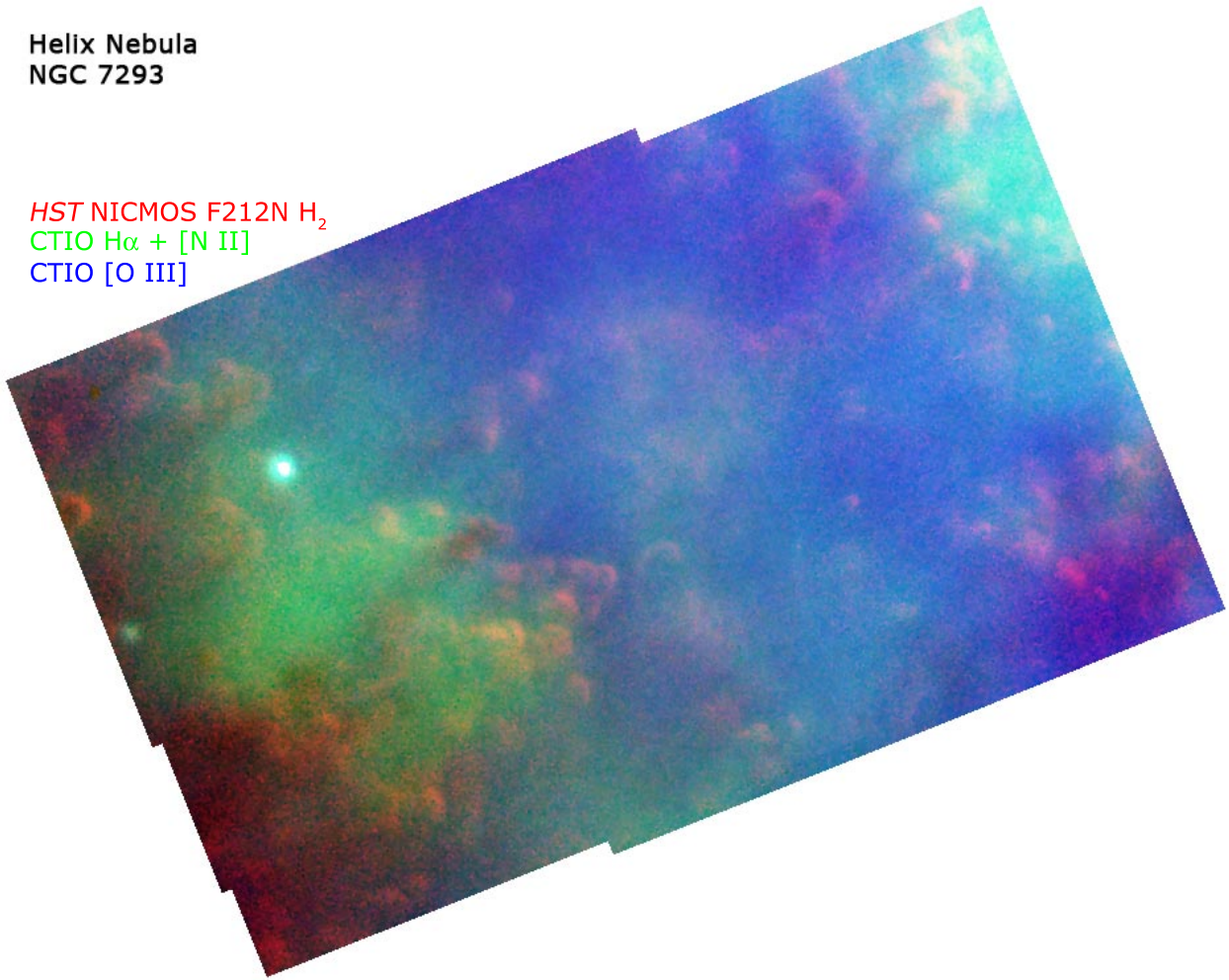


Fig. 9.— NICMOS position 1 in three colors representing the H₂, the H α + [NII] and the [OIII] as shown in the legend. This color comparison re-emphasizes the clumpy nature of H₂ line emission in comparison to the more diffuse ionized gas line emission.

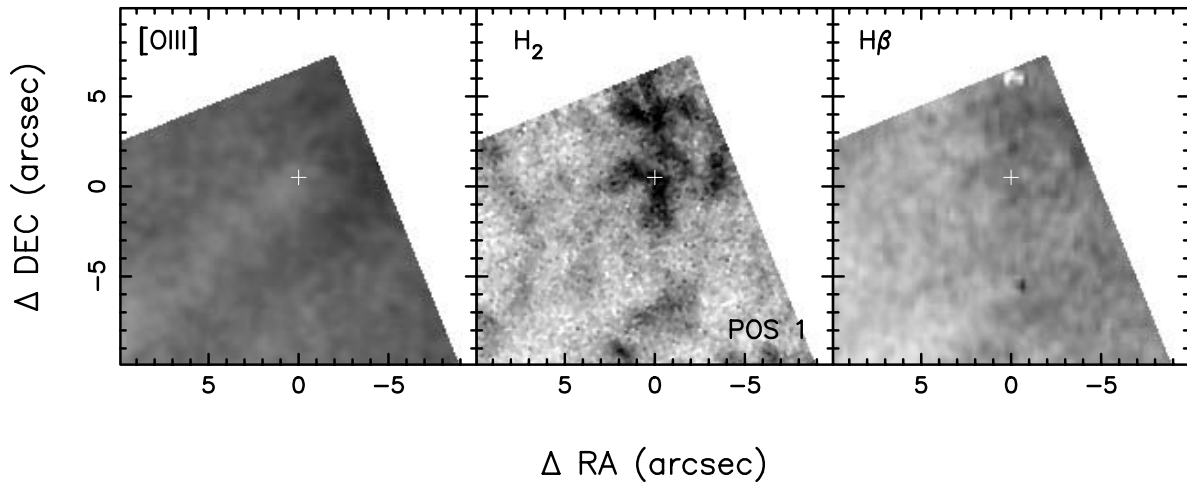


Fig. 10.— The selected H₂ knot from NICMOS position 1 shown in [OIII] (shadow), H₂ and H β line emission. The white cross, which marks the location of the line emission measurement, is a guide for the relative position of these emissions. The H₂ and H β line emissions appear spatially coincident while the [OIII] shadow column ends at the cross and the H₂ arc emission structure.